HHS Public Access

Author manuscript

Nat Cell Biol. Author manuscript; available in PMC 2014 December 01.

Published in final edited form as:

Nat Cell Biol. 2014 June ; 16(6): 574–586. doi:10.1038/ncb2972.

A Trio-Rac1-PAK1 signaling axis drives invadopodia disassembly

Yasmin Moshfegh[*], **Jose Javier Bravo-Cordero**[*], **Veronika Miskolci**, **John Condeelis**, and **Louis Hodgson**[1]

Department of Anatomy and Structural Biology, Gruss-Lipper Biophotonics Center, Albert Einstein College of Medicine of Yeshiva University, Bronx, NY 10461

Abstract

Rho family GTPases control cell migration and participate in the regulation of cancer metastasis. Invadopodia, associated with invasive tumor cells, are crucial for cellular invasion and metastasis. To study Rac1 GTPase in invadopodia dynamics, we developed a genetically-encoded, single-chain Rac1 Fluorescence Resonance Energy Transfer (FRET) biosensor.

The biosensor shows Rac1 activity exclusion from the core of invadopodia, and higher activity when invadopodia disappear, suggesting that reduced Rac1 activity is necessary for their stability, and Rac1 activation is involved in disassembly. Photoactivating Rac1 at invadopodia confirmed this previously-unknown Rac1 function.

We built an invadopodia disassembly model, where a signaling axis involving TrioGEF, Rac1, PAK1, and phosphorylation of cortactin, causing invadopodia dissolution. This mechanism is critical for the proper turnover of invasive structures during tumor cell invasion, where a balance of proteolytic activity and locomotory protrusions must be carefully coordinated to achieve a maximally invasive phenotype.

Introduction

Tumor invasion requires orchestration of actin-based protrusions capable of extracellular matrix (ECM) degradation and cell locomotion[1-3]. Upon epithelial to mesenchymal transformation[4], tumors gain the ability to invade by protruding invadopodia, characterized by their ability to localize matrix metalloproteinases (MMP) important for the proteolytic digestion of ECM [5, 6]. In breast carcinomas, the ability of cells to form invadopodia and

[1]Correspondence should be addressed to: Louis Hodgson, PhD, Department of Anatomy and Structural Biology, Albert Einstein College of Medicine, 1300 Morris Park Avenue, Price 217, Bronx, NY 10461, Louis.hodgson@einstein.yu.edu, Phone 718-678-1027. Fax 718-678-1019.

[*]These authors contributed equally to this work

Authors have no competing financial interests.

Respective Contributions: Y.M. and L.H. designed and built the biosensor. Y.M., J-J.B.C., J.C. and L.H. designed the biological experiments. Y.M., J-J.B.C. and V.M. performed the experiments. J.C. and L.H. advised and gave critical feedback. Y.M. wrote the original manuscript. J-J.B.C. and L.H. revised the manuscript. J-J.B.C., V.M., J.C. and L.H. finalized the manuscript.

their invasive potential are directly correlated [7], thus understanding the molecular mechanisms regulating invadopodia functions is critical.

Cells assemble and protrude invadopodia during invasion[8] and several members of the p21 Rho family of small GTPases, including Cdc42, RhoA, and RhoC, are involved[9, 10]. These GTPases cycle between a GTP-loaded "ON" versus a GDP-loaded "OFF" states [11]. Regulators controlling these states include guanine nucleotide exchange factors (GEF), GTPase activating proteins (GAP), and guanine nucleotide dissociation inhibitors (GDI) [12]. Cdc42 is crucial for invadopodia formation by activating neuronal Wiskott-Aldrich Syndrome protein (N-WASP), upon which other invadopodia core proteins are assembled[13]. RhoC regulates invadopodia integrity by confining actin protrusion within the invadopodium [10]. RhoA is involved in the delivery of MT1-MMP-containing vesicles to degradation sites[10, 14] and other functions associated with the actin cytoskeleton[9]. The mechanism by which these GTPases regulate their respective downstream functions at the invadopodia is spatially distinct [10]. This suggests that the spatiotemporal dynamics of Rho GTPase activations at or surrounding invadopodia are critical, yet not much is known about such dynamics of other Rho isoforms, specifically Rac1. Previous studies indicated Rac1 overexpression and hyperactivity lead to aberrant cell motility and metastatic phenotypes[15-21]. Rac1 was necessary for invasive protrusions in human melanomas[22], and MCF10A breast epithelial cells required Rac1 for TGFβ-dependent matrix degradation[23]. Rac1 was also required for invasion in Ras-transformed melanoblasts[24]. While Rac1 appears to be required for pro-invasive functions in these cases, there is not yet a clear study of Rac1 during invadopodia functions at subcellular scales. A number of studies have begun to address this question[22, 23, 25], and have shown evidence that Rac1 activation may drive invadopodia. However, this has never been directly observed, only indirectly inferred based on traditional experimental methods. Invadopodia are highly regulated and transient sub-cellular structures, and Rac1 has equally fine spatiotemporal activation dynamics within cells[26], making it difficult to accurately study using more conventional approaches.

To address this problem, we developed a fluorescence resonance energy transfer (FRET)-based biosensor for Rac1. The biosensor enables direct visualization of Rac1 activities at subcellular resolution and in time scale of seconds, while maintaining a single-chain structure and correct isoprenylation. Using this biosensor in combination with the focal photo-uncaging of Rac1[27], we report a mechanism by which invasive breast carcinomas disassemble their invadopodia through Trio-Rac1 activation, through cortactin phosphorylation by p21 activated kinase 1 (PAK1). Here we report the involvement of Rac1 in invadopodia turnover, which could be essential in proper regulation of invasive protrusions during invasion and metastasis.

Results

Rac1 restricts matrix-degrading invadopodia activity

To determine the requirement for Rac1 in invadopodia formation and function, we first silenced Rac1 in MTLn3 rat mammary adenocarcinoma cells[28] and assayed for matrix degradation activity[10]. Upon Rac1 depletion[28] (Fig.1a), degradation of extracellular matrix is dramatically increased compared to control siRNA treated cells (Fig.1b&c), suggesting

that Rac1 controls invadopodia activity. This was recapitulated when Rac1 inhibitor NSC23766 was used (Fig.1c&d). This is recapitulated in human MDA-MB231 and BT549 metastatic cell lines [29-31], but not in MCF10A normal human breast epithelial cell line[32] (Supplemental Fig.1a-g). MTLn3 express Rac1 and Rac3, but not Rac2 (Fig.1e). Rac1 RNAi did not affect Rac3 expression levels (Fig.1e), and multiple single siRNA oligonucleotides also resulted in the observed phenotype (Supplemental Fig.1h). Enhanced degradation from Rac1 knockdown was not likely due to lack of cell motion, as the relative invadopodia lifetimes in these conditions were greatly increased, while the average number of invadopodia per cell at any one point in time remained the same (Fig.1d; Supplemental Video 1). These results suggest that Rac 1 activity appears to restrict invadopodia lifetime as well as matrix degrading activity.

A single-chain Rac1 biosensor

Biochemical approaches cannot be used for observing Rac1 activity at invadopodia; we produced a genetically-encoded single-chain Rac1 biosensor. A full-length Rac1 was placed at the C-terminus of the biosensor to maintain the hypervariable region and the correct lipid modification motif, important for plasma membrane and GDI interactions, similar in design to the previous RhoA biosensor[33] (Fig.2a&b). GDI interaction is the main difference to the previous-generation Rac1 biosensor, reflecting the regulatory cycle of Rac1 in sensor readouts[34, 35].

The sensor consists of a monomeric Cerulean, two tandem p21 binding domains (PBD) of PAK1, separated by a structurally optimized 14 amino acid linker chain, monomeric Venus, and full-length Rac1. The tandem PBD allows for autoinhibitory mechanism of PAK1 by maintaining the autoregulatory moiety (amino acids 70-149) [36]. The second PBD contains H83D-H86D GTPase-binding mutations to prevent spurious interactions with other GTPases when the biosensor is activated and the autoinhibition is relieved (Fig.2c).

Since the size of the biosensor precluded *in vitro* purification, we overexpressed it in HEK293 cells and analyzed the fluorescence spectra of mutant versions of the biosensor as previously described[33]. Compared to wild-type (WT), the constitutively active (G12V & Q61L) mutants had a higher emission ratio (FRET/CFP), and the inactive mutants (T17N & T35S) had a reduced emission ratio. Co-expression of 3-fold excess GDI produced a reduced FRET ratio as expected in WT and G12V mutant versions of the biosensor (Fig. 2d&e).

When co-transfected with excess GDI, GEFs that are known to activate Rac1[37] rescued Rac1 activity, while non-Rac1 GEFs did not rescue activity (Fig.2f). Similarly, p50RhoGAP inhibited Rac1 activity, while the control Rap1GAP did not (Fig.2f). These data show the biosensor behaves accurately and is regulated by upstream regulators. The overexpression of G12V and T17N versions of the biosensor in MEFs shows that the in-cell difference in the FRET ratio based on imaging is approximately 40%, similar to the fluorometric analysis (Fig.2g). In versions of the biosensor where both PBDs were mutated (H83D-H86D), FRET was reduced to dominant negative and GDI-inhibited levels (Fig.2h).

Rac1 activity is excluded from invadopodia

We produced an MTLn3 cell line stably incorporating the Rac1 biosensor under tet-OFF regulation to limit the biosensor expression to ≤20% of endogenous Rac1 (Fig.2i) [33, 38]. We stimulated cells with EGF, triggering invadopodia precursor formation[8] and observed Rac1 activity during early events. After stimulation, structures containing cortactin fluorescence appeared and remained throughout the 10-minute duration of imaging, accompanied by a dramatic depletion of Rac1 activity within the invadopodium core (Fig.3a&b; Supplemental Video 2). This exclusion of Rac1 activity was not due to loss of Rac1 from the invadopodia, as endogenous Rac1 or CFP-Rac1 is uniformly distributed (Fig.3c; Supplemental Fig.2a). Similar reduction in Rac1 activity was observed in fixed cells using Cy5-dye labeling cortactin (Fig.3d). MDA-MB-231 cells also show reduced Rac1 activity at invadopodia (Fig. 3e&f). Accumulated cortactin puncta are non-vesicular[39] and degrade matrix (Supplemental Fig.2b&c).

We examined how Rac1 is involved in invadopodia maintenance by observing Rac1 activity in steady-state invadopodia over a period of 3 hours. We began imaging pre-formed invadopodia and examined Rac1 activity throughout their lifetimes. We observed that when stable invadopodium is present, Rac1 activity inside the invadopodium is significantly lower compared to the region just outside (Fig.3b), until when the invadopodium disappears (Fig. 3g; Supplemental Video 3). At this point Rac1 activity is elevated (Fig.3h; Supplemental Fig.2d). This suggests that Rac1 activation could be associated with disassembly of invadopodia. As a control we compared this Rac1 activity profile to RhoA activity[33]. Similar to shown previously for EGF-induced invadopodia [10], steady-state RhoA activity also showed no significant changes (Supplemental Fig.2e).

Focal activation of Rac1 disassembles invadopodia

To test if Rac1 activation triggers invadopodia disassembly, we used photoactivatable Rac1 (PA-Rac1) [27] to activate Rac1 at pre-formed invadopodia and observe how it influences their dynamics. After photoactivation using 1-sec pulses of 457nm light every 30 seconds to MTLn3 cells expressing PA-Rac1 and two invadopodia markers (mTag-RFP-cortactin and GFP-TKS5[40]), the invadopodium that was photoactivated disappears within 6 min of the start of the irradiation, while the un-caged Rac1 produces a lamellipodium protrusion next to the photoactivated region (Fig.4a&c; Supplemental Video 4). Approximately 80% of invadopodia analyzed disappear upon focal photoactivation of Rac1 (Fig.4d). We recapitulated this effect in MDA-MB-231 cells (data not shown). 39% (18/46) of the time there are multiple invadopodia present, and the adjacent invadopodium not directly irradiated disappears at 78% frequency under those conditions. Only 8.7% of invadopodia (4/46) remained when an adjacent invadopodium was irradiated and dissolved. As a control, we used a C450A constitutively caged mutant of PA-Rac1 [27]. In this case photoactivation does not affect the irradiated invadopodium, and approximately 26% of invadopodia dissolved (Fig.4b-d; Supplemental Video 5).

PAK1-cortactin axis propagates Rac1-dependent invadopodia disassembly

Since the evidence pointed to Rac1 inducing invadopodia disassembly, we investigated downstream targets. Two well-studied Rac1 effectors are the PAKs and the WAVE protein

family[18]. Previously WAVE was shown to have no effect on invadopodia[13], but PAK was not studied in this context. High levels of PAK1 are correlated with tumor invasiveness[41]. Previous studies showed that inactive PAK1 is constitutively associated with cortactin independent of Rac1[42], and when activated by a GTPase, PAK1 phosphorylates cortactin on Serine 113, causing the release of cortactin from F-actin[43] to induce turnover of podosomes[44]. As PAK1 is one of the main downstream effectors of Rac1, we hypothesized a direct role in linking Rac1 to invadopodia breakdown. Immunofluorescence indicated endogenous PAK1 co-localizes with cortactin at mature, degrading invadopodia (Fig.5a), even when Rac1 is depleted (Supplemental Fig.3a). Next, we used RNAi against PAK1 (Fig. 5b; Supplemental Fig.1h), recapitulating the results of Rac1 knockdown by increasing matrix degradation (Fig.5c; Supplemental Fig.1a-d). Invadopodia formation was unaffected by PAK1 siRNA, with no change in average invadopodia per cell, while invadopodia lifetime increased (Fig.5d). Collectively, these results implicated PAK1 as the immediate downstream target of Rac1 at the invadopodia to mediate disassembly.

To show if PAK1 is involved in this pathway, we silenced PAK1 and observed invadopodia dynamics upon focal uncaging of Rac1. Uncaging PA-Rac1 in the PAK1 knockdown background did not cause the disappearance of invadopodia (approximately 19% invadopodia disappearance), while producing edge ruffling and a lamellipodium (Fig.5e; Supplemental Fig.3; Supplemental Video 6).

After establishing the Rac1-PAK1-link, we wanted to see if the phosphorylation of cortactin by PAK1 was important. Focal uncaging of PA-Rac1 with an overexpressed mTagRFP-cortactin containing non-phosphorylatable point mutation (S113A) where PAK1 is known to phosphorylate cortactin[43, 45], disassembled the invadopodia only 30% of the time, while the leading edge ruffling and lamellipodia protrusions were unaffected (Supplemental Fig.3b&e; Supplemental Video 7). Expression of the cortactin mutant alone increases matrix degradation similar to depletion of Rac1 or PAK1 (Supplemental Fig.3c), and increases invadopodia lifetime (Supplemental Fig.3d).

Moreover, we used the proximity ligation assay (PLA) between cortactin and phospho-serine to measure the total phospho-serine levels of cortactin at invadopodia demonstrating if the Rac1-PAK1-pathway leads to changes in the total phospho-serine content of cortactin at invadopodia *in situ*. Total cortactin phospho-serine is reduced significantly when PAK1 was silenced, supporting the link between PAK1 and cortactin (Supplemental Fig.3f&g). These results suggest the Rac1-PAK1 pathway likely produces a destabilization of invadopodia structures through serine phosphorylation of cortactin.

TrioGEF activates Rac1 at invadopodia to induce disassembly

Spatial regulation of GTPases is crucial to their function and because they are activated by GEFs, we sought to determine which GEF may activate Rac1 at invadopodia for disassembly. First, we used the Rac1-inhibitor NSC23766, which inhibits Rac1 activation by TrioGEF and Tiam1[46], and performed an invadopodia lifetime study over a 6-hour time period. Untreated cells had average invadopodia lifetimes of 30min [range:14min-2hrs], measured by mTagRFP-cortactin and TKS5-GFP co-localization (Fig.6a; Supplemental Video 8). In NSC23766-treated cells, invadopodia did not disappear during the timeframe of

image acquisition (Fig.6a; Supplemental Video 9). We used another Rac1-inhibitor Z62954982 which inhibits Rac1-Tiam1 interaction but not TrioGEF[47]. The distribution of invadopodia lifetimes was similar to control after the Z62954982-treatment, suggesting that Trio may activate Rac1 at invadopodia (Fig.6a; Supplemental Video 10). Endogenous TrioGEF is localized to invadopodia (Fig.6b), but endogenous Tiam1 does not (Supplemental Fig.4a). No Tiam1-GFP accumulated at invadopodia (Supplemental Fig.4b), and a dominant negative mutant Tiam1[48] did not affect invadopodia functions (Supplemental Fig.4c). Furthermore, silencing TrioGEF (Fig.6c; Supplemental Fig.1h) recapitulates the increase in degradation and invadopodia lifetimes (Fig.6d&e; Supplemental Fig.1a-d), while the average number of invadopodia per cell does not change (Fig.6f), similar to the Rac1 RNAi result. We overexpressed the constitutively activated (Trio-D1SH3) [49] and dominant negative (N1406A-D1407A) of the same Trio-D1SH3[50], and observed that the active form reduced matrix degradation, while dominant negative form produced increased degradation (Fig.6e). Full-length WT, dominant negative (DN), and the short DN Trio-D1SH3 are present in about 20% of invadopodia, while the Trio-D1ΔSH3-dominant negative lacking the tandem SH3 domain cannot localize at invadopodia, and EGF stimulation does not affect the localization of full length Trio (Supplemental Fig.5a-c). Based on this, Trio is recruited transiently to invadopodia through its SH3 domain at DHPH-1 (Supplemental Fig.5d) since less than 30% of invadopodia have Trio accumulation. Moreover, Trio is increased at invadopodia when endogenous Rac1 is silenced (Supplemental Fig.5e), likely as a consequence of its disassembly defect. Trio knockdown lowers the global Rac1 activity levels in cells (Fig.7a&b), making the difference between the inside and outside of invadopodia less pronounced (Fig.7c). Furthermore, we performed PLA under Trio knockdown and found that the total phospho-serine levels on cortactin at invadopodia decreased significantly (Supplemental Fig.3f&g).

An invadopodia-associated complex of cortactin, paxillin and PKC has been shown previously[51], and the GIT1-PIX-PAK complex can be recruited to paxillin through GIT1[52]. PIX proteins are GEF for Rac1 and Cdc42[53]. α- and β-PIX both localize to invadopodia and this recruitment is unaffected by EGF stimulation, however knocking down either of the endogenous PIX isoform reduced the amount of matrix degradation (Supplemental Fig.6a-e). Since this is the opposite phenotype of Rac1, PAK1, or TrioGEF-knockdowns, the PIX proteins are likely involved during other aspects of invadopodia dynamics, but not in disassembly. Moreover, paxillin does not accumulate in the core of the invadopodia, suggesting that PIX localization at invadopodia is not paxillin-mediated (Supplemental Fig. 6f).

Trio-Rac1-PAK1-axis impacts invasion in 3D-environment

The pro-invasive role of Rac1 in aggressive tumors is documented in a number of systems[15-20]. We sought to see if Trio-Rac1-PAK1–axis impacts 3D invasion. Invasion is significantly impacted when Trio, Rac1, or PAK1 is silenced in metastatic tumor cells but not in MCF10A cells (Fig. 8a; Supplemental Fig.1a-f). Motility in 3D-collagen matrices is significantly impaired upon Rac1, PAK1 or Trio depletion (Fig.8b-d). Furthermore, matrix degradation in 3D is increased in absence of the Trio-RAC1-PAK1-axis (Fig.8e&f), suggesting that the same mechanism which aberrantly enhances the matrix degradation in

2D also operates under 3D conditions. These results suggest that proper coordination of matrix degradation and locomotory protrusions is required for efficient invasion in 3D environment.

Discussion

We report the localized activation dynamics of Rac1 directly regulating the stability and disassembly of invadopodia through PAK1 and cortactin phosphorylation in metastatic breast carcinomas (Fig.8g). We show that Trio-GEF activates Rac1 at invadopodia, and this Trio-Rac1-PAK1-cascade is regulated independently from the lamellipodia compartment. This is likely through different immediate downstream effectors, since depleting either Trio or PAK1 did not abrogate EGF-stimulated lamellipodia protrusion, while depleting Rac1 did (Supplemental Fig.7a). Importantly, we provide conserved observations for Trio-Rac1-PAK1-axis in metastatic breast carcinomas but not in normal epithelial cells; a critical distinction in the signaling mechanisms utilized to affect efficient invasions between malignant versus normal cells.

Since invadopodia are transient sub-cellular structures, we approached the problem by building a biosensor for Rac1. The fundamental difference between our sensor and the previous generation system[34] is that the latter is constitutively anchored to the plasma membrane through the k-Ras CAAX box[34, 35], producing GEF-GAP sensors. In our system the sequestration by GDI is correctly taken into account [33].

Our data and other studies, suggested that invasive tumors utilize two separate downstream signaling pathways to achieve efficient migration upon Rac1 activation. The lamellipodia driven by Rac1 is WAVE2-dependent[13, 54]; indeed we show here that in a PAK1-silenced background, photoactivation of Rac1 at an invadopodium does not result in its disassembly, while edge ruffling and lamellipodia protrusions are unaffected. The mechanism by which PAK1 enhances the turnover of invasive processes agrees with other studies suggesting PAK1 inducing the turnover of podosomes[43, 44], and cortactin phosphorylation by PAK destabilizing F-actin – cortactin association[43]. These studies and our results support the idea that Rac1-PAK1-axis induces the turnover of many of these adhesive and invasive processes, including focal adhesions[55-57].

Invadopodia formation is a multistep process [8]. Efficient turnover of invadopodia appears critical to effective invasion. Previously, focal adhesion kinase antagonized c-Src to regulate the total number of invadopodia in MTLn3 cells, thus overexpression of c-Src can produce greater numbers of structures[58]. We show that the number of structures is independently regulated by c-Src [8, 58, 59] and not Trio-Rac1-PAK1-axis (Supplemental Fig.7b&c).

Cancer invasion *in vivo* is a complex process involving localized regulations of signaling proteins, including GTPases. GEFs are established spatial activators of GTPases [37]. Specific mechanism of TrioGEF control is not well known, however we established a role for Trio as the activator of Rac1 at invadopodia. Trio contains two DH-PH domains which target RhoG-Rac1 and RhoA[60]. In glioblastoma, RhoG is involved in invadopodia formation[25]. In breast carcinoma, siRNA of RhoG has no effect on matrix degradation nor does RhoG

accumulate at invadopodia (Supplemental Fig.8). The difference could be because glioblastoma is not derived from epithelium and invades brain tissue locally, thus the ECM environment is much different in brain than epithelium [61]. We showed that the SH3 domain of Trio is required for transient invadopodia localization (Supplemental Fig.5d). These observations clearly point to the importance of localized regulation of GTPases within subcellular compartments; indeed, when TrioGEF was silenced, overall Rac1 activity was reduced by approximately 20% (Fig.7). While this had no effect on EGF-stimulated leading edge protrusion (Supplemental Fig.7a), it clearly impacted invadopodia as both the lifetimes and matrix-degradation were significantly altered. Thus, the functional regulation of how Trio activates Rac1 only at a specific time and in a context of invadopodia disassembly needs to be further explored. Also, other mechanisms may cooperate with the Trio-Rac1-PAK1-axis during turnover of invadopodia[59].

Based on our observations we propose two models where the Rac1-mediated disassembly of invasive protrusions could be advantageous for tumor cells. In 3D invasion *in vivo*, invadopodia and lamellipodia compartments converge into a single leading front[62]. Rac1 activation at the leading front propagates via two separate downstream effector pathways to mediate: 1) disassembly and clearance of components necessary for matrix degradation (through PAK1); and simultaneously, 2) extend protrusions with locomotive characteristics as opposed to degradative (through WAVE2). This is an efficient mechanism for switching between these two characteristics by a single upstream regulator. This model is consistent with reports of Rac1 producing pro-invasive phenotypes[20], because an ability to increase the invadopodia turnover could enhance the ability of tumors to switch rapidly between invasive versus locomotive protrusions. Indeed, cells depleted of Trio-Rac1-Pak1 have motility defects in 3D matrices (Fig.8a-d). Alternatively, invasive cells *in vivo* continuously probe the microenvironment within the ECM to detect regions optimal for invasion[63]. Thus, microenvironmental cues could provide feedback to drive the turnover of degradative protrusions through regulation of localized Rac1 activity modulating the local turnover rates of lamellipodia versus invadopodia. In both models, our observations are consistent with the idea that the turnover of invadopodia is directly regulated through a mechanism activated by Rac1. Under normal conditions, invasive and locomotory protrusions are both cyclical and coordinated, where the end of one is coupled to the start of the other. Thus, when one component is perturbed, the entire cell motility cycle and the invasion machinery become stalled, resulting in aberrantly increased local matrix degradation (Fig.8e&f) but impaired overall invasion and motility in 3D (Fig.8a-d). This coordination is critical to efficient invasion and migration in 3D where all pieces of the system needs to be functional, unlike in stimulated protrusions in 2D where the initial phase of protrusion formation can be unaffected by PAK1 or Trio depletion but not Rac1 (Supplemental Fig.7a). By enhancing the turnover dynamics of invadopodia, Rac1 contributes to efficient cycling of matrix degradation versus locomotory protrusions in invasive tumors, allowing for facile cell migration in 3D.

Materials & Methods

Cell Lines

MTLn3 were cultured and transfected as previously described [10].

MDA-MB-231 (ATCC HTB-26), BT-549 (ATCC HTB-122) were cultured in DMEM with 10% fetal bovine serum (FBS), antibiotics (Invitrogen, Grand Island, NY) and insulin (for BT-549) (Invitorgen) as suggested by ATCC.

MCF10A (ATCC CRL 10317) were cultured following the ATCC protocols. MCF10A were transfected as previously described[23]. MDA-MD-231 and BT-549 were transfected by nucleofection according to manufacturer's protocols (Lonza, Basel, Switzerland). All cell lines mycoplasma tested.

Intramolecular biosensor for rac1

The biosensor for Rac1 was subcloned within the multiple cloning site (MCS) of pTriEX-His-Myc4 (Novagen) between the NcoI and XhoI restriction sites. The construct consisted of the monomeric Cerulean (mCerulean) fluorescent protein[66], BamHI restriction site, two tandem p21-Binding Domains (PBD; a.a. residues 70-149) from PAK1, separated by a HindIII restriction site and GSGGPPGSGGSG linker, monomeric Venus (mVenus) fluorescent protein[67], EcoRI restriction site, a full-length Rac1, and XhoI site immediately following the stop codon. mCerulean was subcloned between the NcoI and BamHI MCS restriction sites using the primer pair 5′- CCATGGTGAGCAAGGGCGAGGAG -3′ and 5′-GGATCCTTTGTACAGCTCGTCCATG 3′. The first PBD was subcloned between the BamHI and HindIII sites using the primer pair 5′-GGATCCAAAGAGCGGCCAGAGATTTCTCT -3′ and 5′-AAGCTTTCCGCCAGACCCTGACTTATCTGTAAAGCTCATGTAT -3′. The second PBD with H83D and H86D GTPase-binding deficient point mutations was subcloned between the HindIII and NotI sites using the primer pair 5′-AAGCTTCCACCAGGGTCTGGAGGCTCCGGGAAAGAGCGGCCAGAGATTTCTCTCC -3′ and 5′- GCTTCCGCTGACTTATCTGTAAAGCTCATG -3′. Point mutagenesis was performed using the Quikchange PCR mutagenesis kit (Stratagene).

mVenus was subcloned between the NotI and EcoRI sites using the primer pair 5′-GCGGCCGCAATGGTGAGCAAGGGCGAGGAGCT -3′ and 5′-CTTGTACAGCTCGTCCATGCCGAATTC -3′. Full-length Rac1 was subcloned between the EcoRI and XhoI sites using the primer pair 5′-GAATTCATGCAGGCCATCAAGTGTGTGG -3′ and 5′-TTACAACAGCAGGCATTTTCTCTCGAG -3′.

For production of the tetracycline-inducible retroviral construct, the entire biosensor cassette was cut out of the pTri-EX backbone using NcoI and XhoI restriction sites, blunt-ended, and ligated into the multiple cloning site of the pRetroX-Tight-Pur vector (Clontech) at the NotI site that was blunt-ended.

The design of the biosensor is such that the built-in binding domain does not compete against the binding of endogenous targets by the activated biosensor (Fig.2c). This feature is critical to reducing potential dominant negative or overexpression artifacts.

Biosensor validation-fluorometry assay

The biosensor expression construct was transfected into LinXE cells plated $8x10^5$ overnight over poly-L-lysine in 6-well plates, using Lipofectamine Plus (Invitrogen) according to manufacturer's protocols. The total amount of DNA was 700ng per well. In cases where biosensor was co-transfected with upstream regulators, the biosensor/GDI ratio was 1:3, and biosensor/GDI/GEF ratio was 1:3:1-2. 48 hours following transfection, cells were fixed with 3.7% formaldehyde in PBS and their fluorescence spectrum was measured using a MicroMax plate reader attached to a Fluororlog MF2 spectrofluorometer (Horiba Jobin Yvonne). Cells were excited at 433nm and a fluorescence emission spectrum was measured between 450-600nm. Background autofluorescence was subtracted from the raw spectra, and normalized to CFP emission at 475nm as previously described[33].

Invadopodia degradation assay

All imaging experiments were performed as previously described [10, 68]. Alexa-568 or -405 conjugated thin gelatin matrix (Invitrogen) was prepared on MatTek dishes (MatTek Corporation) as previously described[69]. Gelatin degradation was measured by quantifying the average area of non-fluorescent pixels per field. Approximately 15 random fields were imaged per condition and each independent experiment was performed at least 3 times and averaged. Invadopodia were identified by cortactin and Tks5 staining and manually counted from images.

Reagents and antibodies

mTagRFP-cortactin has been previously described[8]. Cortactin antibody was purchased from Abcam (Abcam ab33333 clone 0.T.21; used at 1:200). Rac1 (sc-95 clone C-11), PAK1 (sc-882 clone N-20), TrioGEF (sc-28564 clone H-120), Tiam1 (sc-872 clone C-16), β-actin (sc-69879 clone AC-15), β-Pix (sc-136035 clone 23) and α-Pix (sc-10927 clone Q-20) antibodies were purchased from Santa Cruz Biotechnologies. RhoG (04-486 clone 1F3 B3 E5), pSerine (AB1603 polyclonal), Rac2 (07-604 polyclonal) and Rac3 (07-2151 polyclonal) antibodies were purchased from Millipore. mDia1 (610848 clone 51-mDia1) and paxillin (610051 clone 349-Paxillin) antibodies were from BD Transduction Laboratories. All primary antibodies were used at 1:200 dilution. siRNA smart pools for PAK1 (L-091307-02), Trio (L-087912-01), RhoG (L-083717-02), β-Pix (L-098943-02) and α-Pix (L-098102-02) and single oligos for Rac1 (LQ-080171-02), PAK1 (LU-091307-02) and Trio (LU-087912-02) were purchased from Dharmacon, Inc. (Thermo Scientific) or Qiagen (Rac1,: 5′-AAAGAGAUCGGUGCUGUCAAA-3′)[28] and transfected with Oligofectamine (Invitrogen). Human siRNA smart pools for Rac1 (L-003560), Trio (L-005047), PAK1 (L-003521) were purchased from Dharmacon.

NSC23766 was purchased from EMD Biosciences and dissolved in water. Cells were treated with 100μM of the inhibitor before imaging (IC50=50μM) [46, 70]. Rac1 Inhibitor II

(Z62954982) was purchased from EMD Millipore Corporation and dissolved in DMSO. Cells were treated with 25μM of this compound 1 hour before imaging (IC50=12.2μM) [47].

Tiam-1 PH-CC-Ex (a.a. 431-670) competitive inhibitor[48] was PCR amplified from the mouse full length GFP-Tiam-1 by using the primer set 5′-GCCATATATTTGGCCATATTCTCGAGCTCAGGGCACTGTGCGGAAGGCTGGAG-3′ and 5′-GCAATTATATTGACCTAAAGAATTCTTAAGTCCGGGCTGCCACCAGGGCATGA-3′ and ligated into XhoI-EcoRI sites within the multiple cloning site of pEGFP-C1 backbone (Clontech). Tiam-1 catalytically-dead dominant negative mutant (L1200R-L1201S) version was produced by site-directed mutagenesis using the primer pair 5′-GCGCAAACAGCTCCCTGCTCCGAAGCGGGTACTTGAGG-3′ and 5′-CCTCAAGTACCCGCTTCGGAGCAGGGAGCTGTTTGCGC-3′.

TrioGEF dominant negative catalytically dead (N1406A-D1407A) version was produced by site-directed mutagenesis using the primer pair 5′-CTGAGGTGCATGGCAGCAGCGGCTCGCTTCGGCAC-3′ and 5′-GTGCCGAAGCGAGCCGCTGCTGCCATGCACCTCAG-3′.

Full length α-Pix-GFP was a kind gift from Dr. Georg Rosenberger[64].

Full length wildtype c-Src-GFP, constitutively activated Y528F c-Src-GFP and the dominant negative K296R-Y528F c-Src-GFP were a kind gift from Dr. Michael Way [65].

Western blotting

Whole cell lysates were prepared by collecting cells and resuspending in cold lysis buffer (RIPA, plus 4mM PMSF and protease inhibitor cocktail), incubating on ice 30 minutes, then spinning for 30 minutes and collecting the supernatant. Blots were analyzed using the Odyssey Infrared Imaging System (LI-COR, Lincoln, NE). For quantification, the average grey values of bands were measured with ImageJ software.

Stablecell lines

The Tet-inducible Rac1 biosensor-expressing MTLn3 cell line was generated by using GP2-293 packaging cells to produce retrovirus for infection. MTLn3 parental cells were stably transduced under G-418 selection with Retro-X Tet-Off Advanced retroviral vector system (Clontech) as previously described[10]. The Tet-Off MTLn3 cells were transduced again using the retrovirus produced from GP2-293 cells transfected with the pRetroX-Tight-Pur viral vector containing the biosensor within its MCS, and the stable transductants were selected using puromycin at 10μg/mL as previously described[33], in the presence of 2μg/mL doxycylin to repress the biosensor expression. The cells were then FACS sorted to obtain a population of uniform but low biosensor expression levels. For imaging experiments, cells were induced by removing the doxycycline as previously described[33]. Appropriate biosensor expression levels (≤20% of endogenous Rac1) were achieved at 24 hours following the induction. For live-cell imaging, additional constructs, when required, were transiently transfected into induced cells 16 hours prior to start of assays using Lipofectamine 2000 reagent (Invitrogen) following the manufacturer's protocols.

Live cell imaging

MTLn3 cells stably expressing the Rac1 biosensor were induced and transfected with mTagRFP-cortactin[8] and plated on thin gelatin matrix-coated glass coverslips 16 hours before imaging. For EGF-stimulation experiments, cells were starved for 3 hours before image acquisition in L15 medium (Invitrogen) supplemented with .35% BSA, then treated with 5nM EGF for stimulation. Imaging was performed in L15 medium with 5% FBS and Oxyfluor reagent (Oxyrase Inc), in a closed chamber for steady-state experiments.

Rac1 activation levels were measured in living cells by monitoring the ratio of FRET to mCerulean emissions, following previously described methods [33], then mTagRFP-cortactin images were acquired at each time point. Time-lapse sequences were acquired on a custom Olympus IX81ZDC inverted microscope with a beam splitter which enabled simultaneous acquisitions of both FRET and CFP channels using two Coolsnap ESII CCD cameras (Roper Photometrics) mounted on the left side 100% throughput port via an Olympus beamsplitter module, and a set of excitation-emission filterwheels to direct the mTagRFP emission to a third Coolsnap HQII camera (Roper Photometrics) mounted on the bottom 100% throughput port of the microscope. Images were obtained using an Olympus 60X PlanApoN 1.45 NA UIS2 DIC lens and Metamorph software. Filter sets used for the ratiometric imaging were:

mCerulean: ET436-20X, ET480-40M (Chroma Technology); FRET: ET436-20X, ET535-30M (Chroma Technology); mTagRFP: FF585-29, FF628-32 (Semrock).

The primary fluorescence dichroic turret utilized a 10/90 reflection/transmittance mirror (Olympus) that provided the compatibility for all of the bandpass filter sets used. Cells were illuminated with a 100W Hg lamp through a 10% transmittance neutral density filter. At each time point, mCerulean and FRET images were recorded simultaneously for 700ms with binning 2x2. mTagRFP-cortactin image was then acquired with 500ms exposure at 2x2 binning.

Invadopodia lifetime was measured in MTLn3 cells expressing TagRFP-cortactin and TKS5-GFP, plus various experimental conditions. Cells were plated on thin gelatin matrix and imaged for 6 hours with 2 minutes between frames. Lifetime was quantified by measuring the time from appearance of cortactin and TKS5 co-localized spots to time of disappearance.

Image processing

Metamorph software (Molecular Devices) was used to perform image analysis, as previously described[33]. Briefly, images were dark-current, shading-corrected and background-subtracted, followed by a non-linear coordinate transformation in order to achieve a pixel-by-pixel matching of all three camera channels. Binary masks generated through intensity thresholding were applied to each emission channels, and the matched FRET and mCerulean image sets were then ratioed to depict Rac1 activation throughout the cell. A linear pseudocolor lookup table was applied, and the ratio values were normalized to the lower scale value. The ratio was corrected for photobleaching using a previously described approach[33].

Photoactivation

MTLn3 cells were triple-transfected with photoactivatable Rac (PA-Rac) [27] fused to mTagBFP, mTagRFP-cortactin, and TKS5-GFP using Lipofectamine2000, one day before imaging, and plated on thin gelatin-coated glass coverslips overnight. 3nm spots where invadopodia were present were irradiated with 1 second pulses of 457nm light, every 30 seconds. Cortactin and DIC images were acquired every 5 seconds for 10 minutes. Metamorph software was used to measure RFP and GFP intensities.

Invasion Assay

Transwell invasion assay (#354483 BD, bioscience) was performed and analyzed as previously described[10].

Three-Dimensional Motility And Matrix Degradation Assay

Preparation of 3-dimensional cultures was done as previously described[68].

3D motility experiments were performed using a Delta Vision microscope under 20X magnification objective lens and imaged every 5 minutes for 6 hours.

For DQ-collagen degradation experiments, imaging was performed using a Leica SP5 Confocal microscope with a 20X magnification objective lens. Cells were cultured in a mixture of collagen-Matrigel-DQ-collagen 3-matrices for 16 hours prior to fixation and staining with DAPI. Z-stacks of 100 microns depth at 5 micron Z-increments were acquired and the DQ-collagen degradation index was calculated as summation of the mean florescence intensity per Z-slice over the total number of planes per field in the DQ-type I collagen channel.

Proximity Ligation Assay

MTLn3 cells were plated on gelatin matrix, fixed, permeabilized, and stained with primary antibodies for cortactin and pSerine and Phalloidin 488.

The proximity ligation assay was performed according to manufacturer's instructions for the Duolink II Probe anti-rabbit PLUS, PLA probe anti-mouse MINUS, and detection reagent orange (Olink Bioscience, Uppsala, Sweden).

Statistical Analysis

All p-values were determined using a Student *t*-test. No statistical methods were used to pre-determine the sample size, no vertebrate animals were involved. No randomizations were used. The investigators were not blinded to allocation during experiments and outcome assessment. Statistical tests used are stated on every figure legend with p-values as appropriate. Data distribution should meet the normal distribution requirements. No estimate of variation.

Repeatability of experiments—Fig.1a: A representative image is shown from 3 blots.

Fig.1b: Representative image sets are shown from 50 image sets each for the Control and Rac1 siRNA.

Fig.1e: Representative blots are shown from 3blots each condition.

Fig.2c: Representative image from 3 blots.

Fig.2d: Representative fluorometry spectra from 9 wells from 3 independent experiments per condition.

Fig.2g: Representative image set from 4 image sets.

Fig.2i: Representative image from 3 blots.

Fig.3a: Representative timelapse panel is shown from 15 cell movies.

Fig.3c: Representative image set from 17 image sets.

Fig.3d: Representative image set from 22 image sets.

Fig.3e: Representative image set from 10 image sets.

Fig.3g: Representative images are shown from 50 cell movies.

Fig.3h: Representative image sets are shown from 4 cell movies which showed elevated activity of Rac1 prior to invadopodia disappearance. Total steady-state cell movie sets = 50.

Fig.4a: Representative image set is shown from 40 image sets.

Fig.4b: Representative image set is shown from 30 image sets.

Fig.5a: Representative image set is shown from 30 image sets.

Fig.5b: A representative image is shown from 2 blots.

Fig.5c: Representative image set is shown from 40 image sets.

Fig.5e: Representative image set is shown from 27 image sets.

Fig.6b: Representative image set is shown from 41 image sets.

Fig.6c: A representative image is shown from 2 blots.

Fig.6d: Representative image set is shown from 68 image sets.

Fig.7a: Representative image set from 70 image sets.

Fig.8d: Each panel shows 4 representative cell motility traces, out of total of 24 cell traces per each condition.

Fig.8e: Representative image set from 17 image sets for Control condition, from 18 image sets for Rac1 siRNA, from 17 image sets for PAK1 siRNA, and from 19 image sets for Trio siRNA.

Supp. Fig.1a: Representative image set from 40 image sets for Control, from 40 image sets for Rac1 siRNA, from 39 image sets for PAK1 siRNA, and from 41 image sets for Trio siRNA.

Supp. Fig.1c: Representative image set from 29 image sets for Control, from 28 image sets for Rac1 siRNA, from 35 image sets for PAK1 siRNA, and from 31 image sets for Trio siRNA.

Supp. Fig.1e: Representative image set from 40 image sets for Control, from 40 image sets for Rac1 siRNA, from 43 image sets for PAK1 siRNA, and from 40 image sets for Trio siRNA.

Supp. Fig.1g: All blots shown are from single blots.

Supp. Fig.1h: Representative blots are shown from 1 blot for Rac1 panel, 1 blot for Pak1 panel and 2 blots for the TrioGEF panel.

Supp. Fig.2a: Representative image set from 11 image sets.

Supp. Fig.2b: Representative image set from 10 image sets.

Supp. Fig.2c: Representative image set from 12 image sets.

Supp. Fig.2d: Representative image set from 4 image sets showing burst of Rac1 activity.

Supp. Fig.2e: Representative image set from 6 cell movies.

Supp. Fig.3a: Representative image set from 30 image sets.

Supp. Fig.3b: Representative image set is shown from 51 image sets.

Supp. Fig.3f: Representative image set from 46 image sets.

Supp. Fig.4a: Representative image set from 30 image sets.

Supp. Fig.4b: Representative image set from 16 cell movies.

Supp. Fig.5a: Representative image set from 55 image sets for Cortactin-Tks5-Trio-FL-GFP, and from 70 image sets for Cortactin-Tks5-Trio-D1ΔSH3-GFP.

Supp. Fig.5d: Representative image set from 10 cell movies.

Supp. Fig.6a: Representative image set from 9 image sets.

Supp. Fig.6b: Representative image set from 13 image sets.

Supp. Fig.6c: Representative blot from 1 blot each for the α- and β-PIX.

Supp. Fig.6f: Representative image set from 10 image sets.

Supp. Fig.7b: Representative image set from 44 image sets for Cortactin-GFP-control, from 53 image sets for Cortactin-Src-WT-GFP, from 43 image sets for Cortactin-Src-CA-GFP, and 47 image sets for Cortactin-Src-DN-GFP.

Supp. Fig.8a: Representative blot from 1 blot.

Supp. Fig.8b: Representative image set from 9 cell movies.

Supplementary Material

Refer to Web version on PubMed Central for supplementary material.

Acknowledgments

This work was supported by GM093121 (Y.M., J-J.B.C., L.H.), T32GM007491 (Y.M., V.M.), and CA150344 (J.C.). We acknowledge Dr. Georg Rosenberger for providing the α-PIX-GFP construct[64], Dr. Jaap van Buul for providing the Trio constructs[49], and Dr. Michael Way for providing the c-Src constructs[65]. This work is in partial fulfillment of the PhD requirements Y.M. We thank the Dr. John Condeelis, Dr. Jeffrey Segall, Dr. Dianne Cox-lab members for their helpful discussions.

References

1. Fidler IJ. The pathogenesis of cancer metastasis: the ‘seed and soil’ hypothesis revisited. Nat Rev Cancer. 2003; 3:453–458. [PubMed: 12778135]
2. Hanahan D, Weinberg RA. Hallmarks of cancer: the next generation. Cell. 2011; 144:646–674. [PubMed: 21376230]
3. Comen EA. Tracking the seed and tending the soil: evolving concepts in metastatic breast cancer. Discovery medicine. 2012; 14:97–104. [PubMed: 22935206]
4. Thiery JP. Epithelial-mesenchymal transitions in tumour progression. Nat Rev Cancer. 2002; 2:442–454. [PubMed: 12189386]
5. Linder S, Wiesner C, Himmel M. Degrading devices: invadosomes in proteolytic cell invasion. Annu Rev Cell Dev Biol. 2011; 27:185–211. [PubMed: 21801014]
6. Murphy DA, Courtneidge SA. The ‘ins’ and ‘outs’ of podosomes and invadopodia: characteristics, formation and function. Nat Rev Mol Cell Biol. 2011; 12:413–426. [PubMed: 21697900]
7. Coopman PJ, Do MT, Thompson EW, Mueller SC. Phagocytosis of cross-linked gelatin matrix by human breast carcinoma cells correlates with their invasive capacity. Clin Cancer Res. 1998; 4:507–515. [PubMed: 9516943]
8. Oser M, et al. Cortactin regulates cofilin and N-WASp activities to control the stages of invadopodium assembly and maturation. J Cell Biol. 2009; 186:571–587. [PubMed: 19704022]
9. Struckhoff AP, Rana MK, Worthylake RA. RhoA can lead the way in tumor cell invasion and metastasis. Front Biosci. 2011; 16:1915–1926.
10. Bravo-Cordero JJ, et al. A Novel Spatiotemporal RhoC Activation Pathway Locally Regulates Cofilin Activity at Invadopodia. Curr Biol. 2011; 21:635–644. [PubMed: 21474314]
11. Jaffe AB, Hall A. Rho GTPases: biochemistry and biology. Annu Rev Cell Dev Biol. 2005; 21:247–269. [PubMed: 16212495]
12. Etienne-Manneville S, Hall A. Rho GTPases in cell biology. Nature. 2002; 420:629–635. [PubMed: 12478284]
13. Yamaguchi H, et al. Molecular mechanisms of invadopodium formation: the role of the N-WASP-Arp2/3 complex pathway and cofilin. J Cell Biol. 2005; 168:441–452. [PubMed: 15684033]

14. Sakurai-Yageta M, et al. The interaction of IQGAP1 with the exocyst complex is required for tumor cell invasion downstream of Cdc42 and RhoA. J Cell Biol. 2008; 181:985–998. [PubMed: 18541705]
15. Keely PJ, Westwick JK, Whitehead IP, Der CJ, Parise LV. Cdc42 and Rac1 induce integrin-mediated cell motility and invasiveness through PI(3)K. Nature. 1997; 390:632–636. [PubMed: 9403696]
16. Sahai E, Marshall CJ. RHO-GTPases and cancer. Nat Rev Cancer. 2002; 2:133–142. [PubMed: 12635176]
17. Baugher PJ, Krishnamoorthy L, Price JE, Dharmawardhane SF. Rac1 and Rac3 isoform activation is involved in the invasive and metastatic phenotype of human breast cancer cells. Breast Cancer Res. 2005; 7:R965–974. [PubMed: 16280046]
18. Sun D, Xu D, Zhang B. Rac signaling in tumorigenesis and as target for anticancer drug development. Drug resistance updates : reviews and commentaries in antimicrobial and anticancer chemotherapy. 2006; 9:274–287. [PubMed: 17234445]
19. Vega FM, Ridley AJ. Rho GTPases in cancer cell biology. FEBS Lett. 2008; 582:2093–2101. [PubMed: 18460342]
20. Barrio-Real L, Kazanietz MG. Rho GEFs cancer: linking gene expression and metastatic dissemination. Sci Signal. 2012; 5:pe43. [PubMed: 23033535]
21. Fritz G, Just I, Kaina B. Rho GTPases are over-expressed in human tumors. Int J Cancer. 1999; 81:682–687. [PubMed: 10328216]
22. Nakahara H, et al. Involvement of Cdc42 and Rac small G proteins in invadopodia formation of RPMI7951 cells. Genes Cells. 2003; 8:1019–1027. [PubMed: 14750956]
23. Pignatelli J, Tumbarello DA, Schmidt RP, Turner CE. Hic-5 promotes invadopodia formation and invasion during TGF-beta-induced epithelial-mesenchymal transition. J Cell Biol. 2012; 197:421–437. [PubMed: 22529104]
24. Li A, et al. Activated mutant NRas(Q61K) drives aberrant melanocyte signaling, survival, and invasiveness via a Rac1-dependent mechanism. J Invest Dermatol. 2012; 132:2610–2621. [PubMed: 22718121]
25. Kwiatkowska A, et al. The small GTPase RhoG mediates glioblastoma cell invasion. Mol Cancer. 2012; 11:65. [PubMed: 22966858]
26. Kraynov VS, et al. Localized Rac activation dynamics visualized in living cells. Science. 2000; 290:333–337. [PubMed: 11030651]
27. Wu YI, et al. A genetically encoded photoactivatable Rac controls the motility of living cells. Nature. 2009; 461:104–108. [PubMed: 19693014]
28. El-Sibai M, et al. RhoA/ROCK-mediated switching between Cdc42- and Rac1-dependent protrusion in MTLn3 carcinoma cells. Exp Cell Res. 2008; 314:1540–1552. [PubMed: 18316075]
29. Cailleau R, Young R, Olive M, Reeves WJ Jr. Breast tumor cell lines from pleural effusions. J Natl Cancer Inst. 1974; 53:661–674. [PubMed: 4412247]
30. Lasfargues EY, Coutinho WG, Redfield ES. Isolation of two human tumor epithelial cell lines from solid breast carcinomas. J Natl Cancer Inst. 1978; 61:967–978. [PubMed: 212572]
31. Littlewood-Evans AJ, et al. The osteoclast-associated protease cathepsin K is expressed in human breast carcinoma. Cancer Res. 1997; 57:5386–5390. [PubMed: 9393764]
32. Tait L, Soule HD, Russo J. Ultrastructural and immunocytochemical characterization of an immortalized human breast epithelial cell line, MCF-10. Cancer Res. 1990; 50:6087–6094. [PubMed: 1697506]
33. Pertz O, Hodgson L, Klemke RL, Hahn KM. Spatiotemporal dynamics of RhoA activity in migrating cells. Nature. 2006; 440:1069–1072. [PubMed: 16547516]
34. Itoh RE, et al. Activation of rac and cdc42 video imaged by fluorescent resonance energy transfer-based single-molecule probes in the membrane of living cells. Mol Cell Biol. 2002; 22:6582–6591. [PubMed: 12192056]
35. Nakamura T, Kurokawa K, Kiyokawa E, Matsuda M. Analysis of the spatiotemporal activation of rho GTPases using Raichu probes. Methods Enzymol. 2006; 406:315–332. [PubMed: 16472667]

36. Lei M, et al. Structure of PAK1 in an autoinhibited conformation reveals a multistage activation switch. Cell. 2000; 102:387–397. [PubMed: 10975528]
37. Rossman KL, Der CJ, Sondek J. GEF means go: turning on RHO GTPases with guanine nucleotide-exchange factors. Nat Rev Mol Cell Biol. 2005; 6:167–180. [PubMed: 15688002]
38. Machacek M, et al. Coordination of Rho GTPase activities during cell protrusion. Nature. 2009; 461:99–103. [PubMed: 19693013]
39. Desmarais V, et al. N-WASP and cortactin are involved in invadopodium-dependent chemotaxis to EGF in breast tumor cells. Cell Motil Cytoskeleton. 2009
40. Stylli SS, et al. Nck adaptor proteins link Tks5 to invadopodia actin regulation and ECM degradation. J Cell Sci. 2009; 122:2727–2740. [PubMed: 19596797]
41. Whale A, Hashim FN, Fram S, Jones GE, Wells CM. Signalling to cancer cell invasion through PAK family kinases. Frontiers in bioscience. 2011; 16:849–864.
42. Vidal C, Geny B, Melle J, Jandrot-Perrus M, Fontenay-Roupie M. Cdc42/Rac1-dependent activation of the p21-activated kinase (PAK) regulates human platelet lamellipodia spreading: implication of the cortical-actin binding protein cortactin. Blood. 2002; 100:4462–4469. [PubMed: 12453877]
43. Webb BA, et al. Phosphorylation of cortactin by p21-activated kinase. Arch Biochem Biophys. 2006; 456:183–193. [PubMed: 16854367]
44. Webb BA, et al. PAK1 induces podosome formation in A7r5 vascular smooth muscle cells in a PAK-interacting exchange factor-dependent manner. Am J Physiol Cell Physiol. 2005; 289:C898–907. [PubMed: 15944209]
45. Ayala I, et al. Multiple regulatory inputs converge on cortactin to control invadopodia biogenesis and extracellular matrix degradation. J Cell Sci. 2008; 121:369–378. [PubMed: 18198194]
46. Gao Y, Dickerson JB, Guo F, Zheng J, Zheng Y. Rational design and characterization of a Rac GTPase-specific small molecule inhibitor. Proc Natl Acad Sci U S A. 2004; 101:7618–7623. [PubMed: 15128949]
47. Ferri N, Corsini A, Bottino P, Clerici F, Contini A. Virtual screening approach for the identification of new Rac1 inhibitors. J Med Chem. 2009; 52:4087–4090. [PubMed: 19527032]
48. Stam JC, et al. Targeting of Tiam1 to the plasma membrane requires the cooperative function of the N-terminal pleckstrin homology domain and an adjacent protein interaction domain. J Biol Chem. 1997; 272:28447–28454. [PubMed: 9353304]
49. van Rijssel J, Hoogenboezem M, Wester L, Hordijk PL, Van Buul JD. The N-terminal DH-PH domain of Trio induces cell spreading and migration by regulating lamellipodia dynamics in a Rac1-dependent fashion. PLoS ONE. 2012; 7:e29912. [PubMed: 22238672]
50. Debreceni B, et al. Mechanisms of guanine nucleotide exchange and Rac-mediated signaling revealed by a dominant negative trio mutant. J Biol Chem. 2004; 279:3777–3786. [PubMed: 14597635]
51. Bowden ET, Barth M, Thomas D, Glazer RI, Mueller SC. An invasion-related complex of cortactin, paxillin and PKCmu associates with invadopodia at sites of extracellular matrix degradation. Oncogene. 1999; 18:4440–4449. [PubMed: 10442635]
52. Manabe R, Kovalenko M, Webb DJ, Horwitz AR. GIT1 functions in a motile, multi-molecular signaling complex that regulates protrusive activity and cell migration. J Cell Sci. 2002; 115:1497–1510. [PubMed: 11896197]
53. Frank SR, Hansen SH. The PIX-GIT complex: a G protein signaling cassette in control of cell shape. Semin Cell Dev Biol. 2008; 19:234–244. [PubMed: 18299239]
54. Sarmiento C, et al. WASP family members and formin proteins coordinate regulation of cell protrusions in carcinoma cells. J Cell Biol. 2008; 180:1245–1260. [PubMed: 18362183]
55. Manser E, et al. Expression of constitutively active alpha-PAK reveals effects of the kinase on actin and focal complexes. Mol Cell Biol. 1997; 17:1129–1143. [PubMed: 9032240]
56. Frost JA, Khokhlatchev A, Stippec S, White MA, Cobb MH. Differential effects of PAK1-activating mutations reveal activity-dependent and -independent effects on cytoskeletal regulation. Journal of Biological Chemistry. 1998; 273:28191–28198. [PubMed: 9774440]
57. Kiosses WB, Daniels RH, Otey C, Bokoch GM, Schwartz MA. A role for p21-activated kinase in endothelial cell migration. J Cell Biol. 1999; 147:831–844. [PubMed: 10562284]

58. Chan KT, Cortesio CL, Huttenlocher A. FAK alters invadopodia and focal adhesion composition and dynamics to regulate breast cancer invasion. J Cell Biol. 2009; 185:357–370. [PubMed: 19364917]
59. Cortesio CL, et al. Calpain 2 and PTP1B function in a novel pathway with Src to regulate invadopodia dynamics and breast cancer cell invasion. J Cell Biol. 2008; 180:957–971. [PubMed: 18332219]
60. van Rijssel J, van Buul JD. The many faces of the guanine-nucleotide exchange factor trio. Cell Adh Migr. 2012; 6:482–487. [PubMed: 23076143]
61. Wen PY, Kesari S. Malignant gliomas in adults. N Engl J Med. 2008; 359:492–507. [PubMed: 18669428]
62. Bravo-Cordero JJ, Hodgson L, Condeelis J. Directed cell invasion and migration during metastasis. Curr Opin Cell Biol. 2012; 24:277–283. [PubMed: 22209238]
63. Lee K, et al. Matrix compliance regulates Rac1b localization, NADPH oxidase assembly, and epithelial-mesenchymal transition. Mol Biol Cell. 2012; 23:4097–4108. [PubMed: 22918955]
64. Gringel A, et al. PAK4 and alphaPIX determine podosome size and number in macrophages through localized actin regulation. J Cell Physiol. 2006; 209:568–579. [PubMed: 16897755]
65. Newsome TP, Scaplehorn N, Way M. SRC mediates a switch from microtubule- to actin-based motility of vaccinia virus. Science. 2004; 306:124–129. [PubMed: 15297625]
66. Rizzo MA, Springer GH, Granada B, Piston DW. An improved cyan fluorescent protein variant useful for FRET. Nat Biotechnol. 2004; 22:445–449. [PubMed: 14990965]
67. Nagai T, et al. A variant of yellow fluorescent protein with fast and efficient maturation for cell-biological applications. Nat Biotechnol. 2002; 20:87–90. [PubMed: 11753368]
68. Beaty BT, et al. beta1 integrin regulates Arg to promote invadopodial maturation and matrix degradation. Mol Biol Cell. 2013; 24:1661–1675. S1661–1611. [PubMed: 23552693]
69. Chen WT. Proteolytic activity of specialized surface protrusions formed at rosette contact sites of transformed cells. The Journal of experimental zoology. 1989; 251:167–185. [PubMed: 2549171]
70. Yip SC, et al. The distinct roles of Ras and Rac in PI 3-kinase-dependent protrusion during EGF-stimulated cell migration. J Cell Sci. 2007; 120:3138–3146. [PubMed: 17698922]

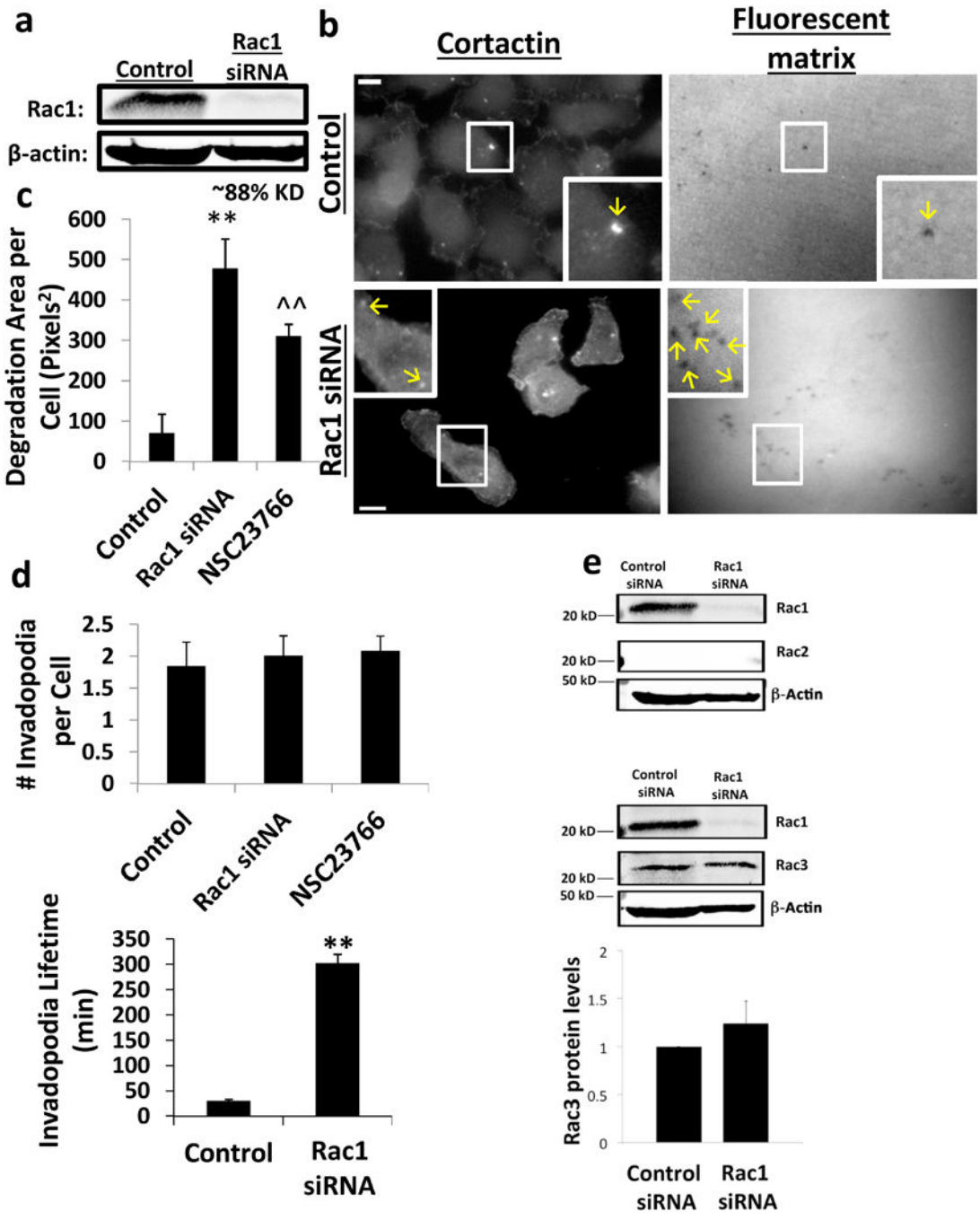

Figure 1. Rac1 depletion increases invadopodia degradation activity

(A) Western blot of cell lysates of control and Rac siRNA treated MTLn3 cells, blotted for Rac1 and β-actin. (B) MTLn3 cells transfected with control siRNA (top panels), or Rac1 siRNA (bottom panels) and plated on Alexa-405 conjugated gelatin overnight. Arrows point to invadopodia and sites of degradation. Scale bar=10μm. (C) Quantification of mean degradation area per cell from (B), including Rac1 inhibitor NSC23766 treatment at 100μM. n=60 fields for each condition, pooled from 5 independent experiments, error bars are S.E.M. Student's t-test was used. **p=0.00022, ^^p=0.011639. (D) Quantification of average

number of invadopodia per cell, and mean invadopodia lifetime from time-lapse movies over a period of 6 hours. Invadopodia lifetime was quantified as the time in minutes from the appearance to the disappearance of RFP-cortactin and TKS5-GFP co-localization spots. n=9 invadopodia for each condition, pooled from 3 independent experiments, error bars are S.E.M. Student's t-test was used. p=0.418134 (#invadopodia per cell Control vs. Rac1 siRNA), p=0.115958 (#invadopodia per cell Control vs. NSC23766), **p=6.531x10-27 (invadopodia lifetime). (E) MTLn3 cells contain Rac1 and Rac3, but not Rac2, and Rac1 siRNA knockdown does not alter the levels of Rac3. Western blot of MTLn3 cells treated with control or Rac1 siRNA and blotted for Rac1, Rac2 and β-actin (top). Western blot of MTLn3 cells treated with control or Rac1 siRNA and blotted for Rac1, Rac3 and β-actin (middle), and quantification of Rac3 protein levels in control and Rac1 knockdown conditions (bottom). n= 3 independent experiments, error bars are S.E.M. Student's t-test was used. p=0.3.

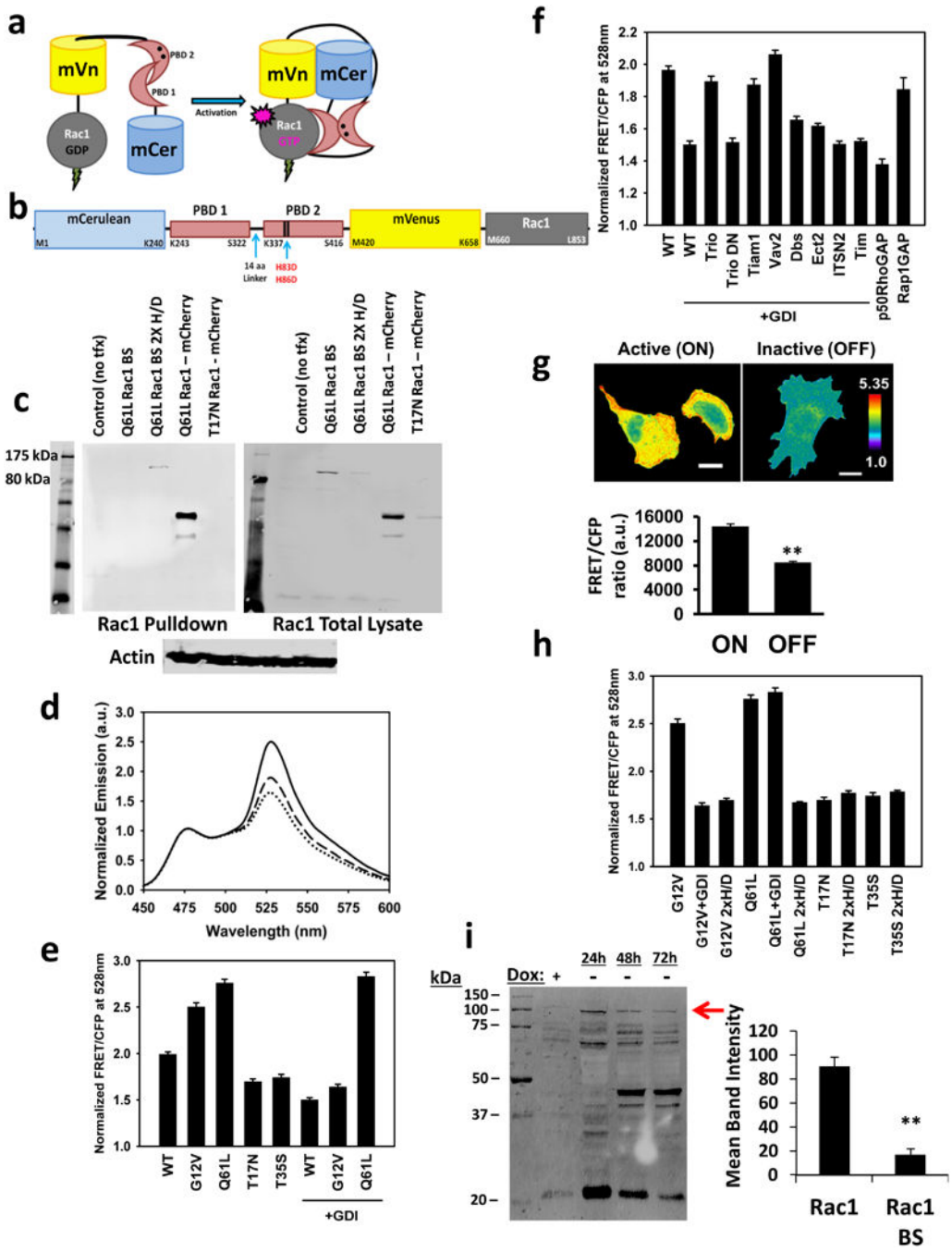

Figure 2. Rac1 biosensor

(A) Biosensor design: inactive (left) vs. active (right). Black dots: H83D-H86D point mutations. (B) Biosensor domains. Amino acid residues are indicated. (C) Rac1 biosensor does not bind endogenous effectors. (Left) GST-PAK-CRIB-pulldown of ~100 kDa constitutively active (Q61L) biosensor, Q61L biosensor with point mutations in both binding domains (2X H-D) and controls, and (Right) total lysates detected for Rac1 and β-actin. (D) Characteristic emission spectra of biosensor mutants (ex: 433nm, normalized to em: 475nm). G12V (active, solid line), T17N (inactive, dashed line), and G12V with 3X-

excess GDI (dotted line) are shown. (E) Ratios of wild-type (WT) and mutant (G12V, Q61L; T17N; T35S-effector-binding-deficient) versions of biosensor, with or without 3X-excess GDI. n=27 wells each condition, pooled from 9 independent experiments, with S.E.M. P values (Student's t-test): WT vs. G12V=$5.49848x10^{-8}$; WT vs. Q61L=$8.92796x10^{-11}$; WT vs. T17N=$6.39471x10^{-5}$; WT vs. T35S=$1.7x10^{-4}$; WT vs. WT +GDI=$5.856x10^{-9}$; G12V vs. G12V+GDI=$1.59632x10^{-10}$; Q61L vs. Q61L+GDI=0.1353. (F) Ratios of wild-type Rac1 biosensor co-expressed with GEF and GAP. Trio, Tiam1 and Vav2 are Rac1 GEFs rescuing biosensor activity under 3X-excess GDI. Trio-DN (dominant negative), Dbs, Ect2, ITSN2, and Tim do not have Rac-GEF activity. p50RhoGAP reduces FRET to GDI-inhibited levels. Rap1GAP is shown as control. n=9 wells each condition, pooled from 3 independent experiments, with S.E.M. P values (Student's t-test): WT biosensor only vs.: WT+GDI=$5.85609x10^{-9}$; Trio=0.07294; Trio-DN=$8.41187x10^{-9}$; Tiam1=0.08062; Vav2=0.01858; Dbs=$8.59088x10^{-7}$; Ect2=$3.51775x10^{-7}$; ITSN2=$1.1627x10^{-8}$; Tim=$3.04742x10^{-8}$; p50RhoGAP=0.009341; Rap1GAP=0.135735. (G) Overexpression of mutant Rac1 biosensors in mouse embryonic fibroblasts. G12V shows higher ratio (Left) than T17N (Right). n=23 cells each condition, pooled from 3 independent experiments, with S.E.M. Scale bars=20μm. **p=$7.27558x10^{-8}$ (Student's t-test). (H) Ratios of G12V & Q61L, T17N, and T35S (effector binding-deficient) mutant versions of the Rac1 biosensor, with and without Rac-binding-deficient mutation in both PBDs (2X H-D). n=9 wells each condition, pooled from 3 independent experiments, with S.E.M. p values (Student's t-test): G12V vs.: G12V+GDI=$1.59632x10^{-10}$; G12V-2xH-D=$6.23298x10^{-9}$; Q61L vs.: Q61L+GDI=0.13529; Q61L-2xH-D=$1.2788x10^{-9}$; T17N vs. T17N-2xH-D =0.04264; T35S vs. T35S-2xH-D=0.136663. (I) Western blot of MTLn3s with tet-OFF Rac1 biosensor and induced for indicated times and detected for Rac1. Red arrow: biosensor band. Optimal induction=24h. Quantification from the 24h-induction lane, showing protein levels of endogenous Rac1 and Rac1 biosensor (Right). **p=0.00086 (Student's t-test), n=3 independent experiments, with S.E.M.

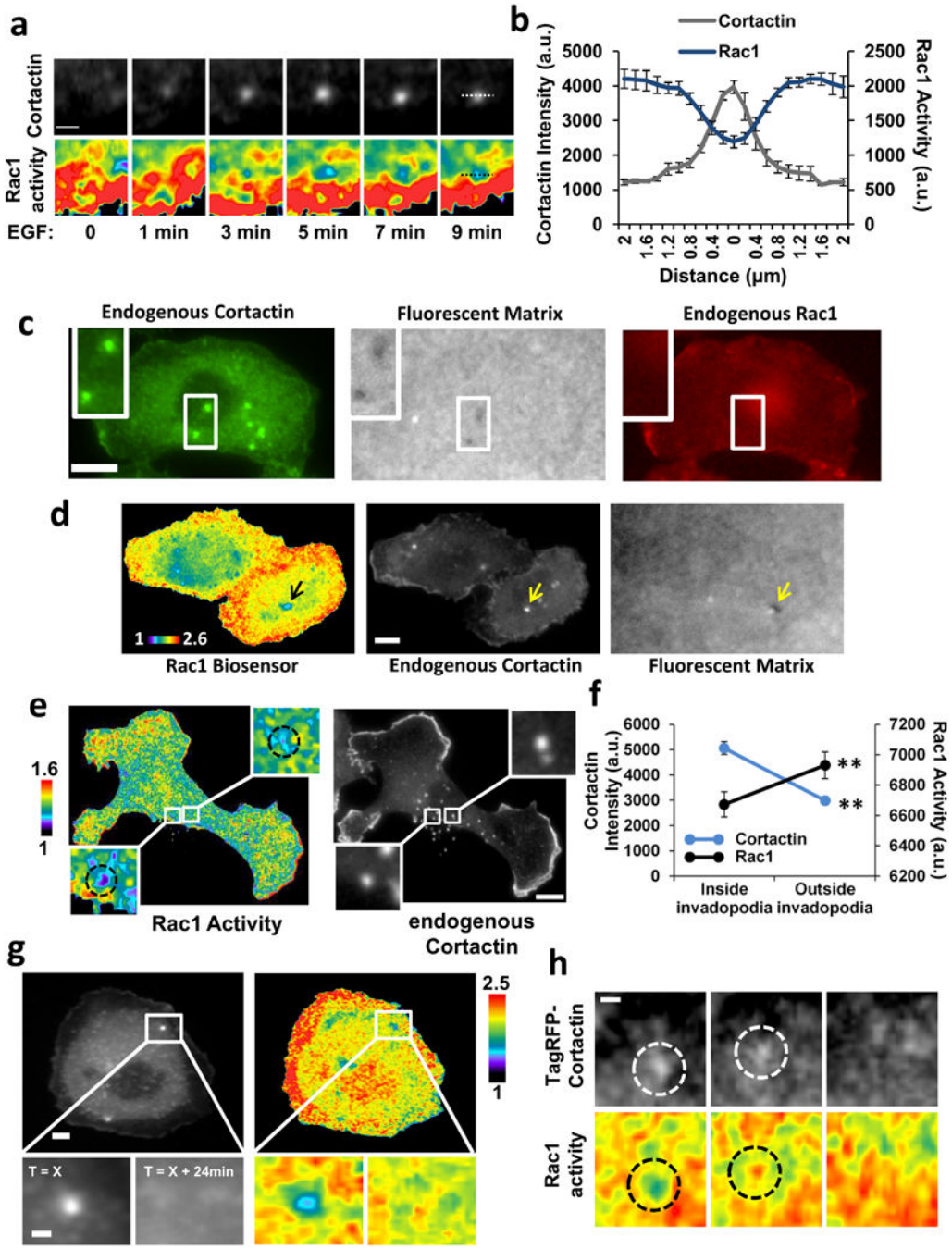

Figure 3. Rac1 activity at invadopodia

(A) Close-up of a single invadopodium forming at specific time-points after EGF stimulation (Supplemental Video 2). Scale bar=2μm. (B) Linescan measurement along invadopodia of Rac1 activity and cortactin fluorescence. Invadopodia measured were approximately 1.3μm in diameter, with small percentage closer to 2 μm. n=27 invadopodia, pooled from 6 independent experiments, with S.E.M. *p=.047 (Student's t-test). The x-axis is the absolute distance measured. The fluorescence data sets were aligned to the maximal center value position of cortactin fluorescence taken as the center of the invadopodia cores.

(C) Rac1 and cortactin antibodies were used to show endogenous localization of each protein. Unlike cortactin, which is concentrated in actively degrading invadopodia (white square insets), endogenous Rac1 (in either GDP- or GTP-bound conformations) is uniformly distributed throughout the cell. Scale bar = 10μm. (D) Rac1 biosensor-expressing MTLn3 cell plated on Alexa 568-conjugated gelatin and stained for cortactin using Cy5 post-fixation to exclude possibilities of spurious FRET between Venus and TagRFP-cortactin. Arrows point to exclusion of Rac1 activity (left) localized to spots of cortactin accumulation (middle) and holes in the matrix (right), indicating a mature, functional invadopodium. Scale bar=10μm. (E) MDA-MB-231 cell expressing Rac1 biosensor and fixed and stained with antibody to endogenous cortactin. Dotted circles show invadopodia location and exclusion of Rac1 activity. Scale bar=10μm. (F) Quantification of cortactin intensity and Rac1 biosensor activity inside and outside cortactin-enriched spots. Rac1 activity is lower inside invadopodia and higher outside, while cortactin accumulation is high inside and low outside. n=19 invadopodia, pooled from 3 independent experiments, with S.E.M. Student's t-test: $^{**}p=1.2486\times10^{-10}$ (cortactin), $^{**}p=2.82709\times10^{-5}$ (Rac1). (G) Representative biosensor-expressing MTLn3 cell at steady-state with TagRFP-cortactin marker. Close-up of pre-formed invadopodium (T=X), and later time point when the invadopodium disappeared (T=X+24min). Scale bar=2μm. (H) Close-up of another invadopodium in its final stages. White and black circles show the invadopodium location and corresponding Rac1 activity levels. (Left) steady-state invadopodia and associated reduced Rac1 activity. (Middle) moment of elevated Rac1 activity at the core of invadopodia just prior to disappearance. (Right) same region after the disappearance of invadopodia. Scale bar=2μm.

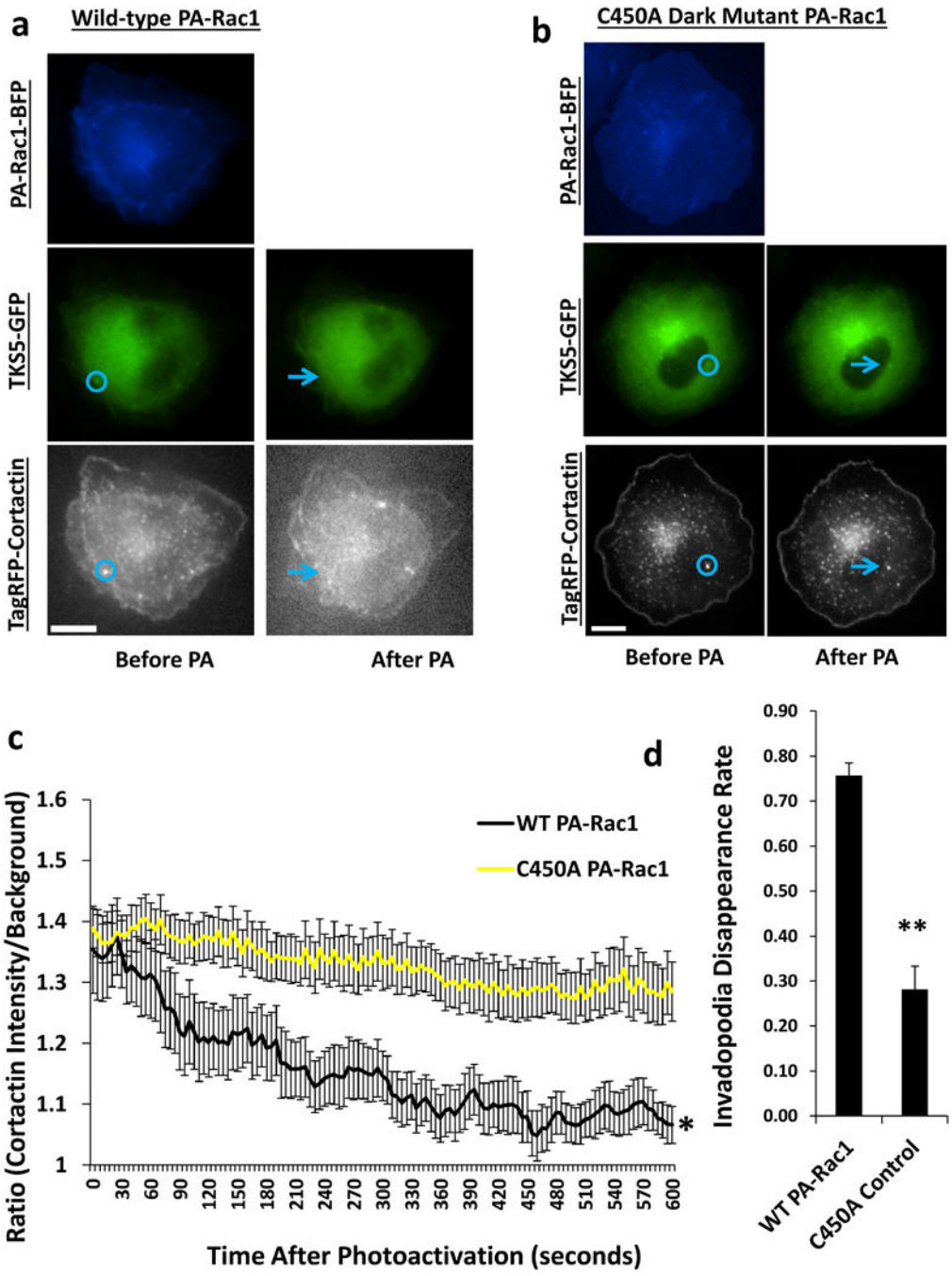

Figure 4. Localized photoactivation of Rac1 induces invadopodia disassembly

(A), (B) Representative images of MTLn3 cell triple-transfected with either PA-Rac1 (A) or C450A PA-Rac1 (B), and two invadopodia markers (TKS5 and cortactin), before and after photoactivation (PA). PA-Rac is uniformly distributed throughout the cells and not specifically concentrated at invadopodia structures, similar to endogenous Rac1 distribution. Blue circles represent photoactivated region. Blue arrows point to same region after photoactivation (from Supplemental Video 4 and 5). Scale Bar= 10μm. (C) Quantification of (A) and (B). n=11 cells for each condition, pooled from 3 independent experiments, error

bars are S.E.M. Student's t-test was used. *p=1.19176x10^{-47}. (D) Quantification of percentage of invadopodia that disappear as a result of photoactivation with wild-type PA-Rac1 and C450A PA-Rac1. n=46 invadopodia (PA-Rac1), pooled from 3 independent experiments, n=19 invadopodia (C450A), pooled from 3 independent experiments, error bars are S.E.M. Student's t-test was used. **p=0.00015175.

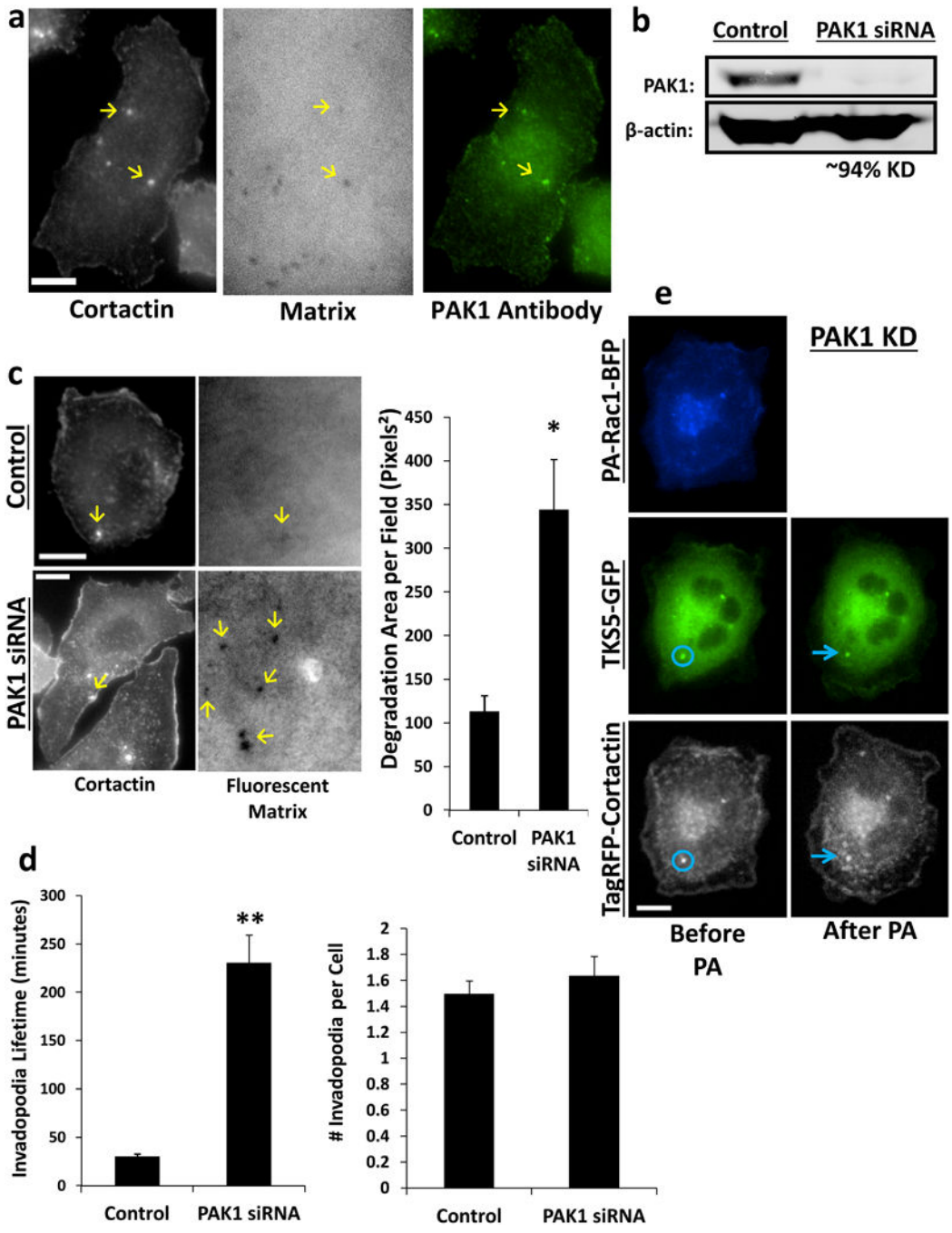

Figure 5. PAK1 links Rac1 to cortactin for invadopodia disassembly

(A) MTLn3 cell plated overnight on Alexa-568 conjugated gelatin and fixed and stained with cortactin or PAK1 antibodies to show endogenous localization. Scale Bar= 10μm. (B) Western blot of cell lysates of control and PAK1 siRNA treated MTLn3 cells blotted for PAK1 and β-actin. (C) MTLn3 cells transfected with control siRNA or PAK1 siRNA and plated overnight on Alexa 568-conjugated gelatin and fixed and stained with cortactin antibody (left). Yellow arrows show mature invadopodia and sites of matrix degradation. Quantification of mean degradation area per field (right). Scale bars = 10μm. n=45 fields for

each condition, pooled from 4 independent experiments, error bars are S.E.M. Student's t-test was used. *p=0.041. (D) Quantification of mean invadopodia lifetime in control and PAK1 siRNA-treated cells, from time-lapse movies over a period of 6 hours (left), and average number of invadopodia per cell (right). Invadopodia lifetime was quantified as the time in minutes from the appearance to the disappearance of RFP-cortactin and TKS5-GFP co-localized spots. n=13 invadopodia for each condition, pooled from 3 independent experiments, error bars are S.E.M. Student's t-test was used. **p=2.883x10-12, p= 0.364372402 (#invadopodia per cell). (E) Representative images of MTLn3 cell transfected with PAK1 siRNA, then triple-transfected with PA-Rac1 and two fluorescent invadopodia markers (cortactin and TKS5) before and after photoactivation (PA) (from Supplemental Video 6). Scale Bar= 10μm.

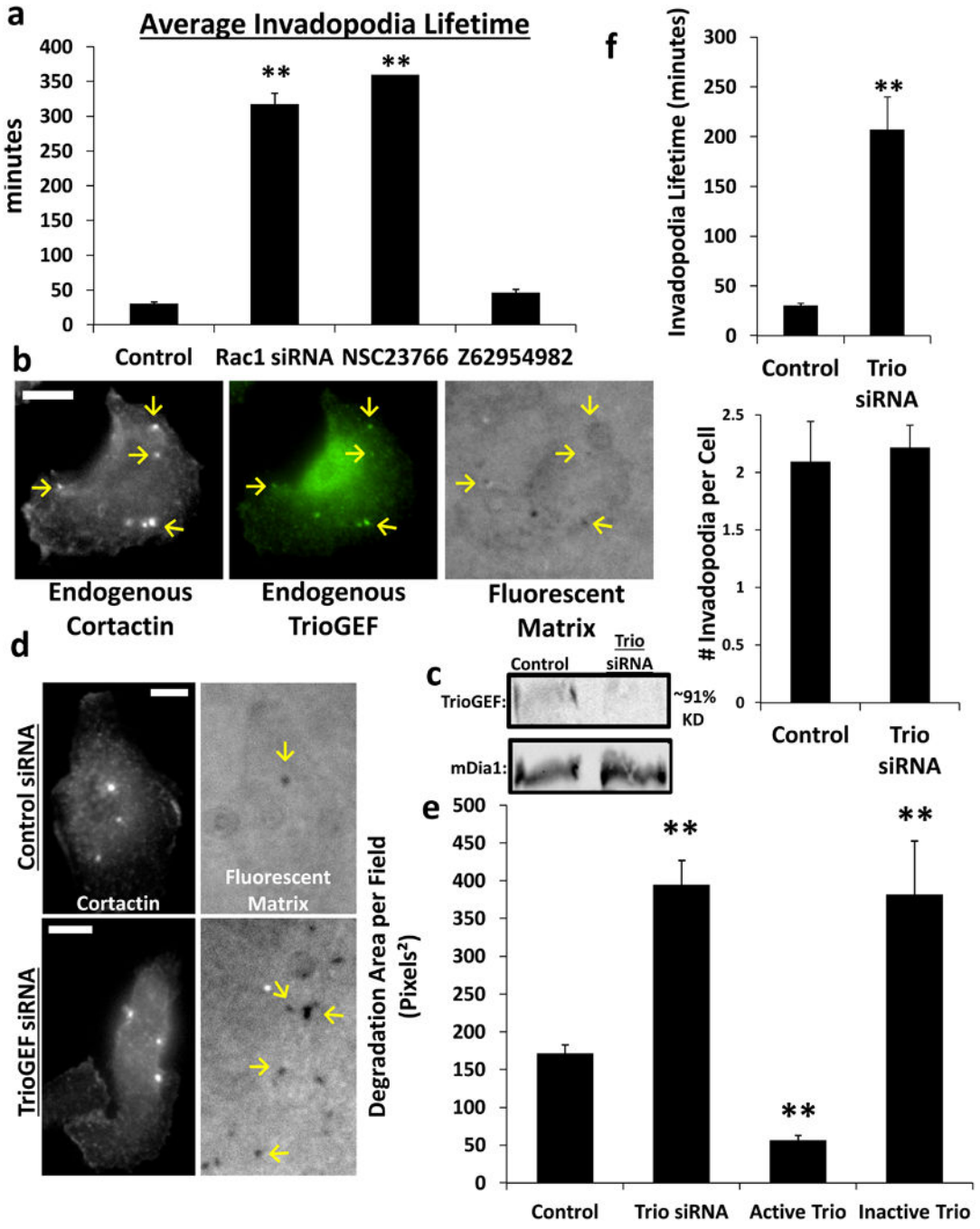

Figure 6. TrioGEF is involved in invadopodia activity

(A) Quantification of invadopodia lifetimes after either depleting Rac1 by siRNA or inhibiting Rac1 with drugs. n=9 invadopodia for each condition, pooled from 3 independent experiments, error bars are S.E.M. Student's t-test was used. **p=6.531x10-27 (Rac1 siRNA), **p≤2.57x10-11 (NSC23766). (B) Representative images of an MTLn3 cell plated overnight on Alexa-405 conjugated gelatin and fixed and stained with cortactin and TrioGEF antibodies to show endogenous localization. Arrows point to mature invadopodia and sites of matrix degradation. Scale Bar= 10μm. (C) Western blot of cell lysates of control

and Trio siRNA treated MTLn3 cells blotted for TrioGEF and mDia1. (D) MTLn3 cells transfected with control siRNA (top panels) or TrioGEF siRNA (bottom panels) and plated on Alexa-405 conjugated gelatin overnight. Arrows point to sites of invadopodia degradation. Scale Bars=10μm. (E) Quantification of mean degradation area per field after TrioGEF depletion or constitutively active or dominant negative mutants of Trio. n=25 fields for each condition, pooled from 3 independent experiments, error bars are S.E.M. Student's t-test was used. **p=4.63x10-7 (Trio siRNA), **p=5.4x10-8 (Active Trio), **p=0.01165 (Inactive Trio). (F) Quantification of mean invadopodia lifetime in control and TrioGEF siRNA-treated cells, from time-lapse movies over a period of 6 hours (top) and average number of invadopodia per cell (bottom). Invadopodia lifetime was quantified as the time in minutes from the appearance to the disappearance of RFP-cortactin and TKS5-GFP co-localized spots. n=11 invadopodia for each condition, pooled from 3 independent experiments, error bars are S.E.M. Student's t-test was used. **p=6.2151x10-10, p= 0.380125939 (#invadopodia per cell).

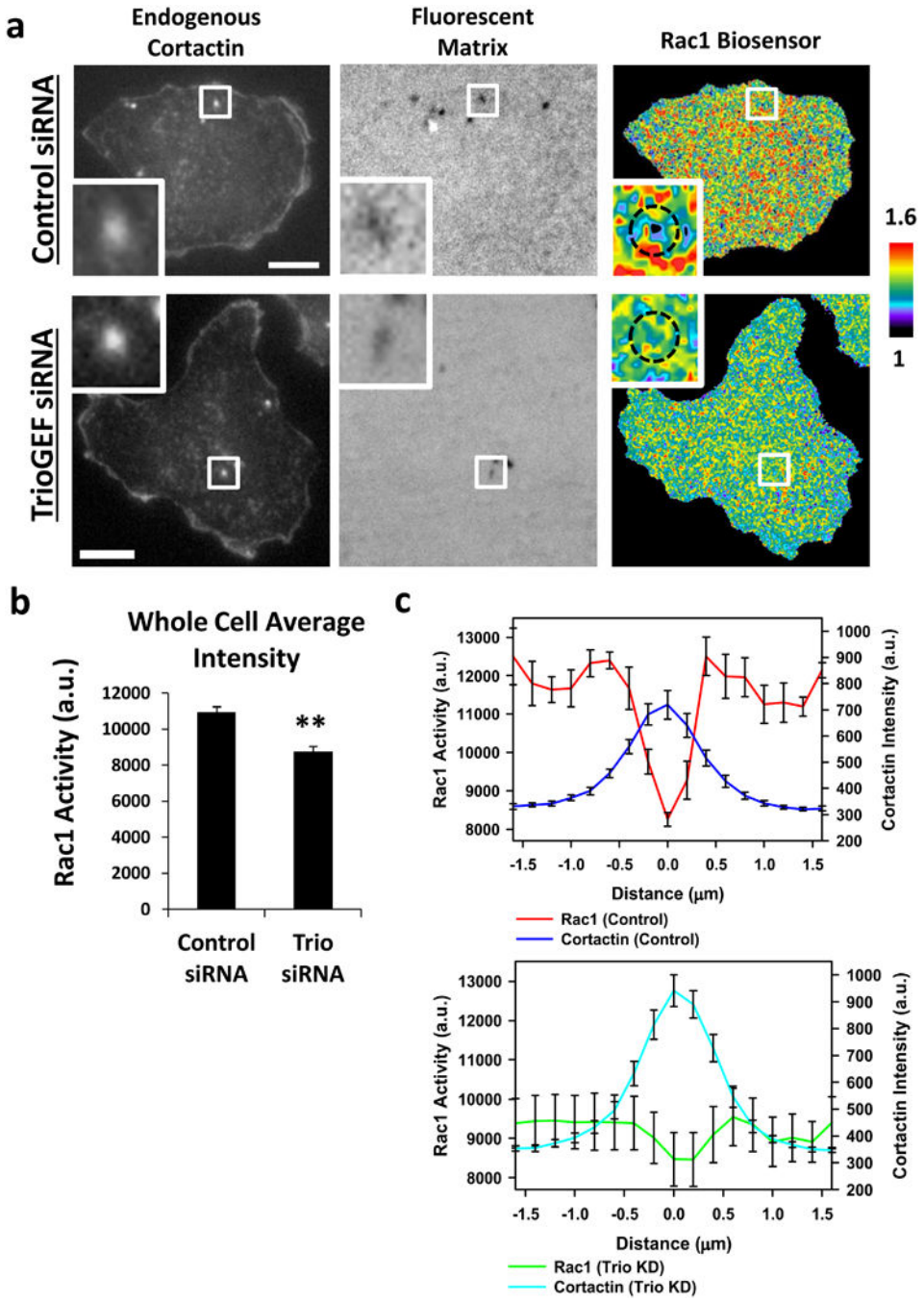

Figure 7. TrioGEF affects Rac1 biosensor activation levels

(A) MTLn3 cell expressing Rac1 biosensor and treated with Control or Trio GEF siRNA plated on Alexa-405 conjugated gelatin and fixed and stained for endogenous cortactin. White squares are magnified (bottom panels) to show a mature, degrading invadopodium. Black circle points to Rac1 activity corresponding to the invadopodium. Scale bars=10μm. (B) Quantification of average whole-cell Rac1 biosensor activity in control and TrioGEF RNAi-depleted cells. Knocking down Trio causes Rac activity levels to drop outside of the invadopodia. n=18 cells each condition, pooled from 3 independent experiments, error bars

are S.E.M. Student's t-test was used. **p=1.50643x10^{-5}. (C) Quantification of cortactin intensity in relation to Rac1 biosensor activity at invadopodia in control and TrioGEF siRNA-treated cells. n=14 invadopodia for each condition, pooled from 3 independent experiments, error bars are S.E.M. Student's t-test was used. p = 3.1981x10^{-10}, comparing the average Rac1 activity levels outside the invadopodia between the control versus the TrioGEF knockdown.

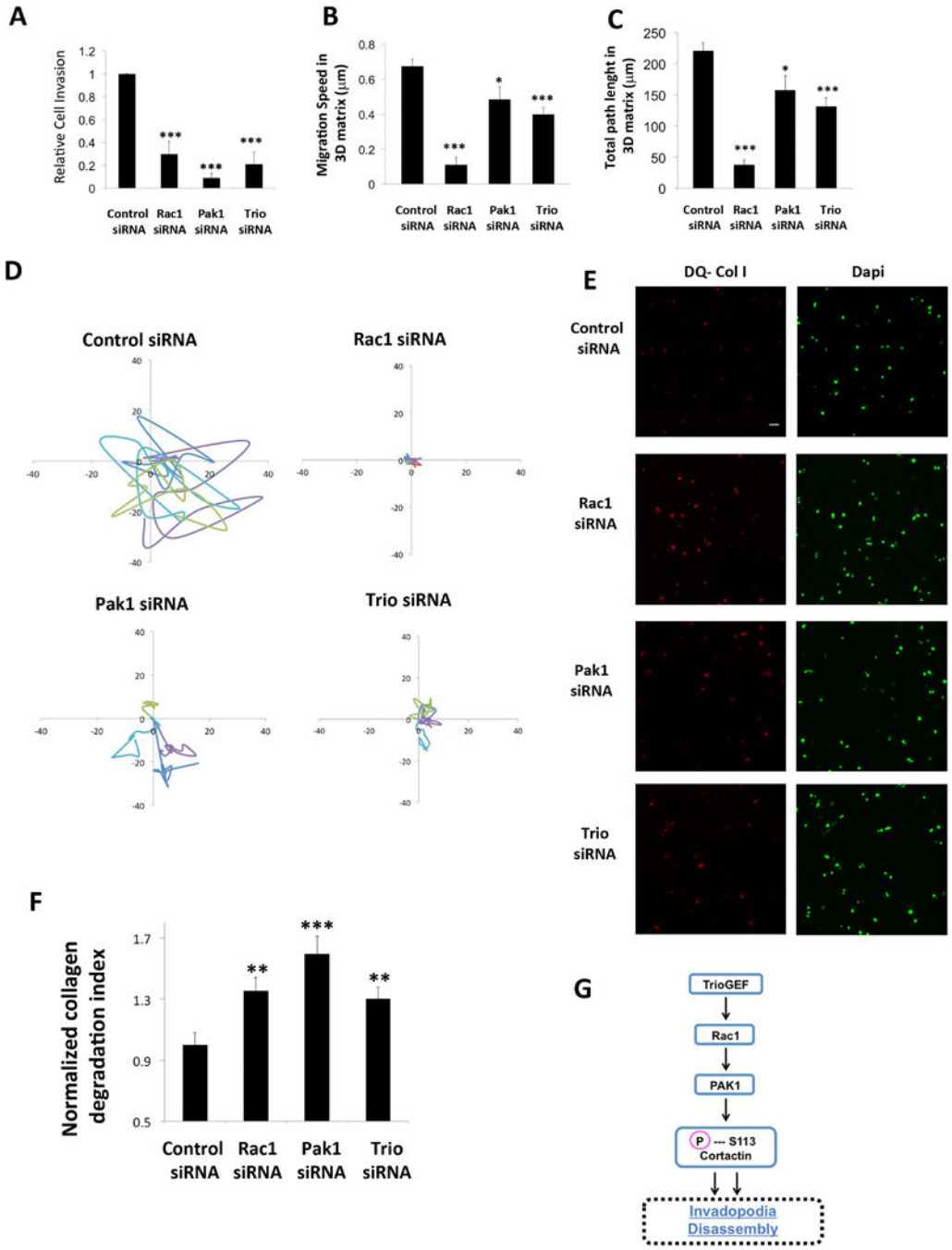

Figure 8. Trio-Rac1-PAK1 signaling axis is necessary for efficient invasion and 3D motility

(A) MTLn3 cells transfected with control, Rac1, PAK1 and Trio siRNA show reduced invasion through matrigel. n= 12 fields, pooled from 3 independent experiments per condition, error bars are S.E.M. Student's t-test was used. ***p= 0.00065 (Rac1), ***p= $5.2x10^{-7}$ (PAK1), ***p= 0.00039 (Trio). (B) MTLn3 cells transfected with control, Rac1, PAK1 and Trio siRNA show reduced migration speed in 3D matrices. n= 24 cells from one experiment per condition were analyzed, error bars are S.E.M. Student's t-test was used. ***p= $1.88x10^{-15}$ (Rac1), ***p= $1.32x10^{-5}$ (Trio), *p= 0.022 (PAK1). (C) MTLn3 cells

transfected with control, Rac1, PAK1 and Trio siRNA show reduced total distance migrated by cells by cells over time in 3D matrices. n= 24 cells from one experiment per condition were analyzed, error bars are S.E.M. Student's t-test was used. ***p= $7.86x10^{-16}$ (Rac1), ***p= $2.24x10^{-5}$ (Trio), *p= 0.023 (PAK1). (D) Representative plots of x–y displacement (in μm) of 4 individual cell traces of cells moving in 3D matrices. (E) Representative images of the maximum projections of 100μm stacks of MTLn3 cells treated with Trio, Rac1, or PAK1 siRNA and embedded in a 3D collagen-matrigel matrix containing DQ-Collagen. DQ-Col I intensity and DAPI staining is shown. Scale bar = 50μm. (F) Quantification of mean DQ-collagen (degradation) per field in MTln3 cells treated with control, Rac1, PAK1 or Trio siRNA. n = 16 fields per condition, pooled from 3 independent experiments, error bars are S.E.M. Student's t-test was used. **p= 0.0059 (Rac1), ***p= 0.00017 (PAK1), **p= 0.009 (Trio). (G) Model for the regulation of invadopodia turnover. In order for invadopodia to disassemble Rac1 needs to be activated by TrioGEF. Downstream of Rac1, PAK1 phosphorylates cortactin at S113, releasing cortactin and presumably mediating the destabilization of the F-actin filaments, disassembling the local actin cytoskeleton and ultimately the invadopodium structure.